Electronic Supplementary Material (ESI) for Journal of Materials Chemistry C.

Three new polymorphs of 1,8-diacetylpyrene: a material with packing-dependent luminescence properties and a testbed for Crystal Structure Prediction Supporting Information

Daniel Tchoń, David Bowskill, Isaac Sugden,
Piotr Piotrowski and Anna Makal,
contact: *amakal@chem.uw.edu.pl*

December 22, 2020

Contents

Chapter S1

Methods

S1.1 Crystallizations

Crystallization solutions were prepared at room temperature by placing ≈ 5 mg of 2"AP in 2 mL glass vials, adding 100 μL of solvent and vortexing at 3000 rpm for a few seconds. In case of a lack of solubility, another 100 μL of solvent was added and vortexing was repeated. Final solutions contained 1 mL of acetonitrile, 1.5 mL of methanol, 100 μL of chloroform and 100 μL of anisole accordingly. Additionally, two ≈ 2 mg samples of 2"AP were placed in separate 2 mL glass vials, dissolved in 0.5 mL of acetonitrile and 0.75 mL of methanol accordingly and 200 μL of n-hexane was placed on top of these solution. The samples were left for the solvent to evaporate.

Crystallizations from anisole, acetonitrile / n-hexane and chloroform / n-hexane mixtures yielded selectively α form. Crystallizations from acetonitrile alone or anisole / n-hexane mixture yielded predominantly 2"AP-α with traces of β in the form of extremely thin tiny plates. Crystallizations from chloroform and methanol with or without n-hexane yielded selectively 2"AP-β as thick dark-yellow plates.

Crystals of 2"AP-γ and 2"AP-δ polymorphs could be obtained exclusively by pressurization of the 2"AP-α in quasi-hydrostatic conditions in a Diamond Anvil Cell, yielding single-crystal to single-crystal transformation. In both instances phase transitions were fully reversible and a single crystal of 2"AP-α could be retrieved once atmospheric pressure was restored. 2"AP-γ could only be obtained with very rapid pressure increase, i.e.: from atmospheric to ≈ 1 GPa in a single step (i.e. in less than 30 s) and hence was more difficult to obtain, especially in a DAC where pressure was increased by manual tightening the screws. More gradual pressurization of 2"AP-α led consistently to 2"AP-δ polymorph. Obtaining of either 2"AP-γ or 2"AP-δ did not depend on a pressure-transmitting media used in our experiments (either Paratone-N or silicone oil).

S1.2 Melting point determination

Determination of the melting point temperatures was performed for single crystals of the polymorphs of 2"AP available at atmospheric pressure. The purity and quality of each crystal was confirmed by a short X-ray diffraction experiment (unit cell determination). Similarly-sized single crystals were placed on a siliconized glass wafer

on a LinkamScientific TMS94 hot stage and then slowly heated at a rate of 2°C/min in air under a microscope. Such procedure was repeated twice on fresh single crystals. The 2"AP-β consistently melted first at ca. 157°C, while meting of 2"AP-α occurred at ca. 162°C, in agreement with earlier studies [Rajagopal et al., 2014].

S1.3 High-pressure experiments

High-pressure experiments utilized multiple Diamond Anvil Cells (DACs) of either modified Merrill & Bassett [Merrill and Bassett, 1974] or DACOne20 design, the latter used mainly in the case of 2"AP-β diffraction studies. The main difference between these two designs is the aperture angle, which in the second case is significantly larger. DACs utilized in spectroscopic experiments were also tested for inherent diamond fluorescence to assure that it would not affect sample measurements. The tests in all cases revealed insignificant response to excitation beam.

Pressure estimation utilized fluorescence from reference ruby spheres, one of which was inserted into DAC alongside the sample in each high pressure experiment. The ruby signal was identified using an Almax Optiprexx PLS spectrometer, affording the nominal precision of 0.05 GPa. Position of the R1 peak was determined by the means of fitting a pseudo-Voigt curve to the fluorescence spectrum using custom-made software pRuby. [Tchoń and Makal, 2021]. The pressure was then estimated based on calibration curve determined by Piermarini et al. [Piermarini et al., 1975]. Temperature correction was also applied. [Ragan et al., 1992] The R1 shift was in each case estimated relative to a reference point, which was measured using the same ruby inside DAC at the beginning or at the end of respective study.

Table S1.1: *Parameters of DACs utilized in performed high pressure experiments.*

	Modified Merrill-Bassett	DAC One20
Diameter of diamond cullet	0.75 mm	0.50 mm
Diameter of gasket hole	0.50 mm	0.30 mm
Nominal opening angle	40°	60°
Effective opening angle	30–35°	45–50°

Effective DAC opening angle cutoffs, smaller then the nominal aperture were used for the sake of data processing, as the intensities of the few reflections registered beyond the effective limits were found to be heavily affected by gasket shadowing.

S1.4 X-ray data collection

XRD data collection was performed using CrysAlisPRO version 1.171.38.46, according to the description provided in the main text. Since high data completeness could not be obtained in some high-pressure cases, experimental strategies involved exposition times up to 400 seconds per frame and multiple redundant runs to assure that collected data will be of best possible quality. A summary of obtained unit cell parameters and other experiment descriptors are listed in Tables S1.2 and S1.3.

Table S1.2: *Data reduction and refinement details for 2″AP-α, γ and δ.*

Crystal data								
Sum formula, M_r	$C_{20}H_{14}O_2$, 286.31							
Symmetry information	monoclinic, $P2_1/c$, Z=4, Z'=1							
Crystal phase	α	α	γ	γ	γ	δ	δ	δ
Pressure \ GPa	0.00	0.34(10)	0.84(10)	1.16(1)	1.65(10)	0.88(10)	0.98(10)	2.12(10)
a \ Å	8.13770(10)	8.109(3)	8.072(3)	7.997(3)	8.045(4)	8.288(2)	8.250(2)	8.2093(19)
b \ Å	22.9058(3)	22.807(5)	22.714(12)	22.591(8)	22.756(10)	21.531(9)	21.62(10)	21.333(7)
c \ Å	7.23590(10)	7.27(2)	7.106(11)	6.94(3)	6.80(4)	7.213(9)	7.166(2)	6.973(8)
β \ °	93.7010(10)	93.12(11)	92.98(7)	92.73(14)	93.1(2)	98.93(5)	98.87(3)	99.07(5)
V \ Å^3	1345.96(3)	1343(4)	1301(2)	1253(6)	1243(8)	1271.6(17)	1263(6)	1205.8(15)
Density \ g cm^{-3}	1.413	1.416	1.462	1.518	1.531	1.496	1.506	1.577
Data collection								
Temperature	100.00(10)	295	293(2)	293(2)	293(2)	296.1(7)	293(2)	296.2(4)
Radiation type	micro-focus sealed X-ray tube							
Wavelength \ Å	0.71073	0.56087	0.56087	0.56087	0.56087	0.56087	0.56087	0.56087
Absorption correction	Empirical multi-scan (SCALE3 ABSPACK)							
μ \ mm^{-1}	0.090	0.058	0.060	0.062	0.062	0.061	0.061	0.064
Tmin	0.61121	0.27698	0.06509	0.00708	0.07587	0.15978	0.82644	0.81465
Tmax	1.00000	1.00000	1.00000	1.00000	1.00000	1.00000	1.00000	1.00000
Diffractometer	Rigaku Oxford Diffraction SuperNova							
Resolution \ Å	0.442	0.780	0.904	0.781	0.837	0.830	0.801	0.830
Reflections: measured	115754	4077	861	1454	1451	5304	2063	4747
independent	16246	821	533	607	528	1188	579	1064
observed	13010	611	271	380	308	514	350	536
h range	$[-18, 18]$	$[-10, 10]$	$[-8, 8]$	$[-10, 10]$	$[-9, 9]$	$[-9, 9]$	$[-10, 9]$	$[-9, 9]$
k range	$[-51, 51]$	$[-28, 29]$	$[-23, 12]$	$[-20, 25]$	$[-22, 24]$	$[-24, 24]$	$[-5, 5]$	$[-24, 24]$
l range	$[-14, 16]$	$[-3, 4]$	$[-4, 3]$	$[-3, 3]$	$[-3, 3]$	$[-5, 5]$	$[-8, 8]$	$[-5, 5]$
Rint	0.0459	0.0605	0.0906	0.0396	0.0846	0.2050	0.0741	0.1138
Rsigma	0.0277	0.0636	0.1451	0.0633	0.1040	0.2061	0.1067	0.1515
Completeness to 0.83Å	100.0%	29.7%	22.5%	24.6%	23.4%	51.3%	24.3%	48.3%
Refinement								
R1	0.0752	0.1399	0.2024	0.1441	0.2230	0.2165	0.1413	0.1819
R1 ($I > 2\sigma$)	0.0590	0.0971	0.1208	0.0975	0.1558	0.0958	0.0659	0.0794
wR2	0.1535	0.2272	0.3526	0.2964	0.3986	0.2589	0.1409	0.1974
wR2 ($I > 2\sigma$)	0.1452	0.2045	0.2866	0.2547	0.3561	0.1922	0.1149	0.1542
GooF (restrained)	1.136	1.064	0.908	0.966	1.050	1.050	1.000	1.045
No. of parameters	201	177	201	175	175	201	201	201
No. of restraints	0	165	291	208	353	0	189	6
$\Delta\rho_{max}$ \ eÅ^{-3}	1.679	0.159	0.318	0.271	0.432	0.251	0.089	0.189
$\Delta\rho_{min}$ \ eÅ^{-3}	-0.335	-0.128	-0.277	-0.211	-0.400	-0.238	-0.098	-0.200
$\Delta\rho_{rms}$ \ eÅ^{-3}	0.079	0.034	0.073	0.059	0.120	0.064	0.025	0.048

Table S1.3: *Data reduction and refinement details for 2"AP-β.*

Crystal data								
Sum formula, M_r	$C_{20}H_{14}O_2$, 286.31							
Symmetry information	orthorhombic, $Fdd2$, Z=8, Z'=0.5							
Crystal phase	β	β	β	β	β	β	β	β
Pressure \ GPa	0.00	0.72(10)	1.00(10)	1.29(1)	1.57(10)	1.64(10)	1.87(10)	2.03(10)
a \ Å	4.69175(9)	4.5651(17)	4.5674(17)	4.5691(17)	4.5836(11)	4.464(8)	4.5345(14)	4.545(3)
b \ Å	35.5546(5)	35.55(9)	35.23(9)	34.74(9)	34.10(6)	34.87(11)	34.26(7)	34.45(15)
c \ Å	16.2326(3)	16.071(5)	16.111(6)	15.984(5)	16.062(4)	15.923(7)	16.040(5)	16.010(8)
V \ Å^3	2707.81(8)	2608(7)	2592(7)	2537(7)	2511(4)	2479(9)	2492(6)	2506(11)
Density \ g cm^{-3}	1.405	1.458	1.467	1.499	1.515	1.534	1.527	1.518
Data collection								
Temperature	100.00(10)	284(11)	290.6(10)	291.3(3)	291.3(3)	293(2)	293(2)	291.2(4)
Radiation type	micro-focus sealed X-ray tube							
Wavelength \ Å	0.71073	0.71073	0.71073	0.71073	0.71073	0.56087	0.71073	0.71073
Absorption correction	Empirical multi-scan (SCALE3 ABSPACK)							
μ \ mm^{-1}	0.090	0.093	0.094	0.096	0.097	0.063	0.098	0.097
Tmin	0.827	0.79464	0.65734	0.80931	0.79559	0.78945	0.37716	0.56306
Tmax	1.00000	1.00000	1.00000	1.00000	1.00000	1.00000	1.00000	1.00000
Diffractometer	Rigaku Oxford Diffraction SuperNova							
Resolution \ Å	0.476	0.831	0.727	0.822	0.729	0.902	0.860	0.925
Reflections: measured	31142	2321	2279	1540	2015	713	2008	1248
independent	6521	631	683	552	659	366	500	381
observed	4903	293	471	244	454	222	327	214
h range	$[-8, 9]$	$[-5, 5]$	$[-6, 5]$	$[-5, 5]$	$[-6, 5]$	$[-4, 4]$	$[-5, 5]$	$[-4, 4]$
k range	$[-69, 74]$	$[-18, 19]$	$[-18, 18]$	$[-17, 17]$	$[-17, 18]$	$[-22, 29]$	$[-18, 18]$	$[-16, 15]$
l range	$[-33, 33]$	$[-19, 19]$	$[-21, 21]$	$[-19, 19]$	$[-21, 21]$	$[-17, 17]$	$[-18, 18]$	$[-16, 16]$
Rint	0.0490	0.1286	0.0726	0.1272	0.0528	0.0775	0.1406	0.1851
Rsigma	0.0449	0.1141	0.0675	0.1364	0.0620	0.1278	0.1308	0.1144
Completeness to 0.83Å	99.5%	53.5%	52.3%	49.5%	51.4%	39.8%	47.4%	34.5%
Refinement								
R1	0.0939	0.1706	0.0981	0.1685	0.0871	0.1475	0.1373	0.1471
R1 ($I > 2\sigma$)	0.0691	0.0675	0.0612	0.0580	0.0518	0.0865	0.0897	0.0981
wR2	0.1657	0.2116	0.1241	0.1735	0.1012	0.1988	0.2351	0.2618
wR2 ($I > 2\sigma$)	0.1527	0.1511	0.1097	0.1154	0.0871	0.1594	0.1972	0.2193
GooF (restrained)	1.084	1.025	1.078	0.940	1.040	0.941	1.042	1.140
No. of parameters	101	101	101	101	101	89	100	101
No. of restraints	1	79	79	79	1	145	85	79
$\Delta\rho_{max}$ \ eÅ^{-3}	1.297	0.166	0.091	0.137	0.103	0.171	0.187	0.168
$\Delta\rho_{min}$ \ eÅ^{-3}	-0.298	-0.176	-0.120	-0.154	-0.105	-0.173	-0.209	-0.176
$\Delta\rho_{rms}$ \ eÅ^{-3}	0.093	0.046	0.030	0.040	0.028	0.050	0.063	0.054

S1.5 Deposition

Structures mentioned in this paper were deposited as individual entries within Cambridge Structural Database. [Groom et al., 2016] The deposition numbers assigned to these 2 structures of 2"AP-α, 8 structures of 2"AP-β, 3 structures of 2"AP-γ and 3 structures of 2"AP-δ are between 2039408 and 2039423. Exact deposition number for each structure have been presented in Table S1.4.

Table S1.4: *CCDC deposition numbers of crystal structures investigated in these studies, sorted by crystal phase and exerted pressure.*

Polymorph	Pressure	CCDC deposition number
2"AP-α	atmospheric	2039413
	0.34 GPa	2039408
2"AP-β	atmospheric	2039409
	0.72 GPa	2039410
	1.00 GPa	2039412
	1.29 GPa	2039411
	1.57 GPa	2039414
	1.64 GPa	2039415
	1.87 GPa	2039419
	2.03 GPa	2039422
2"AP-γ	0.84 GPa	2039418
	1.16 GPa	2039420
	1.65 GPa	2039421
2"AP-δ	0.88 GPa	2039416
	0.98 GPa	2039423
	2.12 GPa	2039417

S1.6 Photographs

The micrographs were taken using Olympus SZX16 stereoscopic microscope, equipped in motorized XY-stage. The photographed samples were illuminated either with UV (365 nm) or visible light. The VL-6 UV lamp removed from the CN-6 Vilber darkroom was used as an external UV source.

S1.7 Crystal Structure Prediction

In all cases, the molecule was first geometry minimized in the gas phase at the PBE0/6-31G(d,p) level of theory using Gaussian [Frisch et al., 2016]. Flexible torsion angles were determined through second derivatives and finite difference perturbations. Local approximate models (LAMs) were constructed by using a uniform

grid along the DOFs, at 120° increments, before running the adaptive LAM algorithm [Sugden et al., 2016] until converged to 5 kJ/mol accuracy, at the same level of theory.

Refinement of the crystal structure landscape of 2"AP was carried out using CrystalOptimizer [Kazantsev et al., 2011]. Multipoles up to rank 4 were generated using GAUSSIAN [Frisch et al., 2016] and GDMA with the PBE0 6-31G(d,p) level of theory. For the repulsion/dispersion potential, a novel set of transferable parameters were tested. These parameters were generated using the newly developed CrystalEstimator [Bowskill et al., 2021, Bowskill et al., 2020] software, using DFT optimized crystal structures as reference data. The parameters were derived to be consistent with the multipole-based calculations at the PBE0/6-31G(d,p) level of theory, and are applied at the CrystalOptimizer stage.

In CrystalEstimator, optimal parameter values (Table S1.5) are estimated by minimizing the discrepancy between model optimized crystal geometries and energies, with respect to some reference data. In this case, the reference data contains optimal crystal structures and energies for a variety of hydrocarbons, oxy-hydrocarbons, and azo-hydrocarbons. Both the optimal geometries and energies are obtained from DFT-D calculations in VASP (version 5.4) using the TPSS function with the D3 correction. An energy cut off of 1000 eV was used for the plane waves. The Brillouin zone was sampled using a Gamma centered Monkhorst–Pack approximation at k-point grids separated by approximately $0.025 \times 2\pi$ Å^{-1}. Crystal structures were relaxed with this model allowing the unit cell volume as well as the atomic positions to optimize. Structural relaxations were halted when the calculated force on every atom was less than 0.01 eV Å^{-1}.

Table S1.5: *Optimal transferable parameters determined by CrystalEstimator.*

Atom site 1	Atom site 2	A \ eV	B \ Å	C \ eVÅ^6
C	C	3640.77	0.277777778	25.26
C	H	374.36	0.272479564	4.58
C	O	3379.62	0.264550265	17.03
C	N	2360.76	0.271002710	22.14
H	H	113.58	0.267379679	1.47
H	O	280.90	0.259740260	2.62
H	N	395.57	0.265957447	2.53
O	O	878.91	0.252525253	6.38
O	N	452.22	0.258397933	11.85
N	N	7603.01	0.2645502650	22.36

In total, 71 crystal structures were used in the fitting process. For this fitting, the A and C parameters of the Buckingham potential for each pairwise interaction type are estimated explicitly without use of combining rules. The electrostatic model used in combination with the Buckingham potential is a multipole based model, which is also generated at the PBE0 6-31G(d,p) level of theory for consistency with model used in CrystalOptimizer[Kazantsev et al., 2011].

S1.8 Other Theoretical Calculations

A series of calculations using dispersion-corrected DFT and 6-31G** basis set were performed in CRYSTAL17 with a tight k-point grid with at most $0.026 \times 2\pi$Å^{-1} between k-points. [Dovesi et al., 2018] Values of band gaps, lattice energy and conformational energy (also called conformational stress in the text) were calculated. Crystal structures of 2"AP polymorphs in pressure range up to 6GPa (85% to 105% of experimental unit cell volume) as well single molecule geometry have been optimized. In all cases strict truncation criteria for the Coulomb and Exchange sums (10^{-7}, 10^{-7}, 10^{-7}, 10^{-7}, 10^{-29}) were applied to ensure proper convergence of the calculations. Some of the aforementioned calculations were also performed in VASP v5.4.4 [Hafner, 2008] using the TPSS functional and D3 dispersion correction. The RMSD between lowest-pressure experimental and VASP-optimized structures of 2"AP-α, β, γ and δ amounts to 0.076, 0.076, 0.116 and 0.108, respectively. Further details regarding methodology of these calculations can be found in CSP section of this document as well as in the main text.

In order to obtain values of lattice energy, defined as a difference between energy of optimized bulk containing one molecule and free molecule, periodic calculations assuming temperature of 0K and pressure of 0GPa were performed. The value was obtained as a sum of conformational and cohesive components. Conformational component was defined as a difference between energy of optimized bulk (per molecule) and energy of single molecule with bulk-derived geometry. Value of conformational stress was defined as a difference between energy of 2"AP molecules with bulk-derived geometry and optimized in vacuum.

Table S1.6: *Alternative version of Table 2 from the main text, presenting 2"AP energy values obtained from aforementioned DFT calculations in CRYSTAL17. All values are given in kJ mol^{-1}, recalculated to one molecule of 2"AP.*

Structure	$E_{\text{cohesive, no BSSE corr}}$	$\Delta E_{BSSEcorr}$	E_{cohesive}	$E_{\text{conformational}}$	E_{lattice}
2"AP-α	-239.8	+61.3	-178.5	+6.0	-172.5
2"AP-β	-239.5	+61.9	-177.6	+4.5	-173.1
2"AP-γ	-240.3	+62.3	-178.0	+5.6	-172.4
2"AP-δ	-244.5	+63.0	-180.5	+9.3	-171.2

High-pressure crystal structures of 2"AP-β, γ and δ were obtained using CRYSTAL's EOS option, [Erba et al., 2014] where the optimization for ten evenly spaced unit cell volumes was performed automatically. Despite numerous attempts, during this process geometry of α polymorph always inevitably drifted towards crystal structure of 2"AP-δ and the calculations diverged. A series of optimizations in pressure range up to 2GPa was performed manually, but as seen on Figures S5.1 or S5.7 the geometry and electron structure still appears to converge to that of 2"AP-δ.

Table S1.7: *Detailed results of fitting theoretically optimized bulk structures of 2"AP-β, γ and δ to Vinet equation of state, [Vinet et al., 1987] rescaled to one molecule in each case. Values corresponding to the most stable polymorph in given conditions were emphasized, while those corresponding to the second most stable polymorph were underlined. For graphical representation see Figure 5 in main text.*

Structure	2"AP-β	2"AP-γ	2"AP-δ
$V_0 \setminus$ Å^3	1263.8216	1234.9344	1238.3292
$E_0 \setminus$ AU	-3682.71590832	-3682.71402667	-3682.71422151
$B_0 \setminus$ GPa	17.62	17.94	18.07
$B_0' \setminus 1$	7.87	8.22	7.84
$E(0.0GPa)$ /AU	**-3682.71590832**	-3682.71402667	-3682.71422151
$E(0.5GPa)$ /AU	**-3682.71413340**	-3682.71232799	-3682.71251934
$E(1.0GPa)$ /AU	**-3682.70965956**	-3682.70805665	-3682.70821203
$E(1.5GPa)$ /AU	**-3682.70329784**	-3682.70199360	-3682.70206846
$E(2.0GPa)$ /AU	**-3682.69553184**	-3682.69460120	-3682.69455187
$E(2.5GPa)$ /AU	**-3682.68667606**	-3682.68617879	-3682.68596563
$E(3.0GPa)$ /AU	-3682.67694794	**-3682.67693256**	-3682.67652056
$E(3.5GPa)$ /AU	-3682.66650478	**-3682.66701128**	-3682.66636977
$E(4.0GPa)$ /AU	-3682.65546414	**-3682.65652629**	-3682.65562827
$E(4.5GPa)$ /AU	-3682.64391692	**-3682.64556314**	-3682.64438485
$E(5.0GPa)$ /AU	-3682.63193456	**-3682.63418926**	-3682.63270982
$E(6.0GPa)$ /AU	-3682.60688360	**-3682.61041568**	-3682.60828017
$E(7.0GPa)$ /AU	-3682.58065838	**-3682.58553219**	-3682.58268129
$E(8.0GPa)$ /AU	-3682.55350106	**-3682.55976671**	-3682.55615263
$E(9.0GPa)$ /AU	-3682.52558794	**-3682.53328512**	-3682.52886876
$E(10.0GPa)$ /AU	-3682.49705176	**-3682.50621207**	-3682.50096113

Chapter S2

Structure description

S2.1 Phase transitions of 2"AP-α

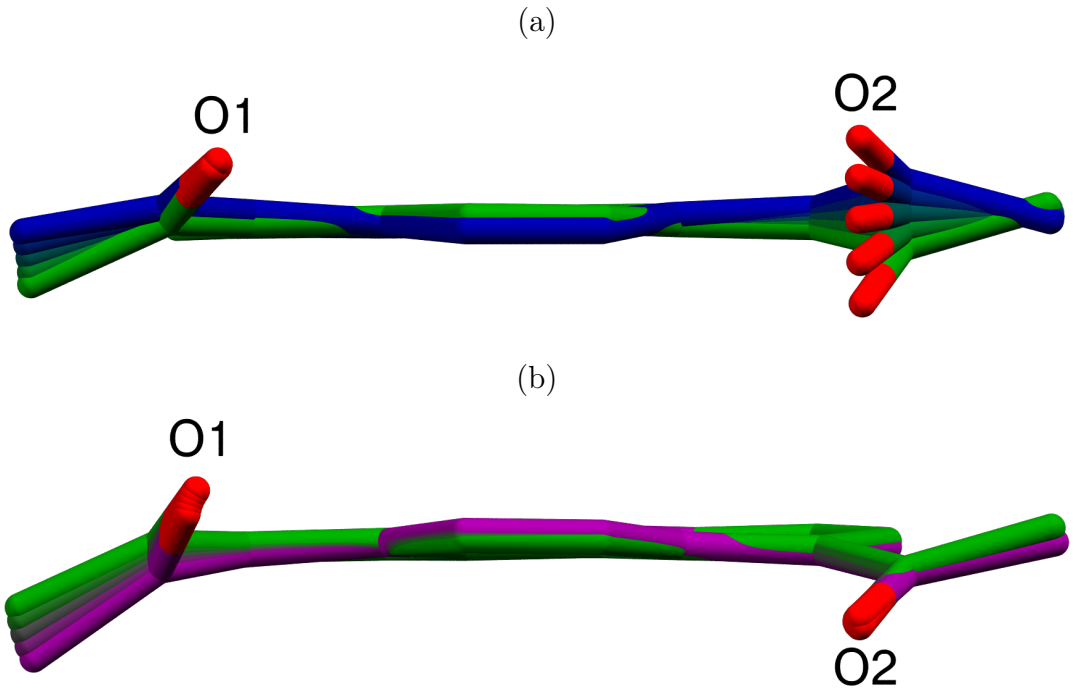

Figure S2.1: *Change of side chain conformation between single molecules of polymorphs a) α (green) and γ (blue); b) α and δ (purple), with intermediate structures introduced to guide the eye. Phase transfer to 2"AP-γ, while more optical energy-wise, is accompanied by a significant structural changes, due to the conformation switching from* cis *to* trans*. Meanwhile, kinetically favoured transition to 2"AP-δ is accompanied only by a minor rotation of δ_1.*

S2.2 Comparison of 2"AP-α, 2"AP-β with optimized free molecule

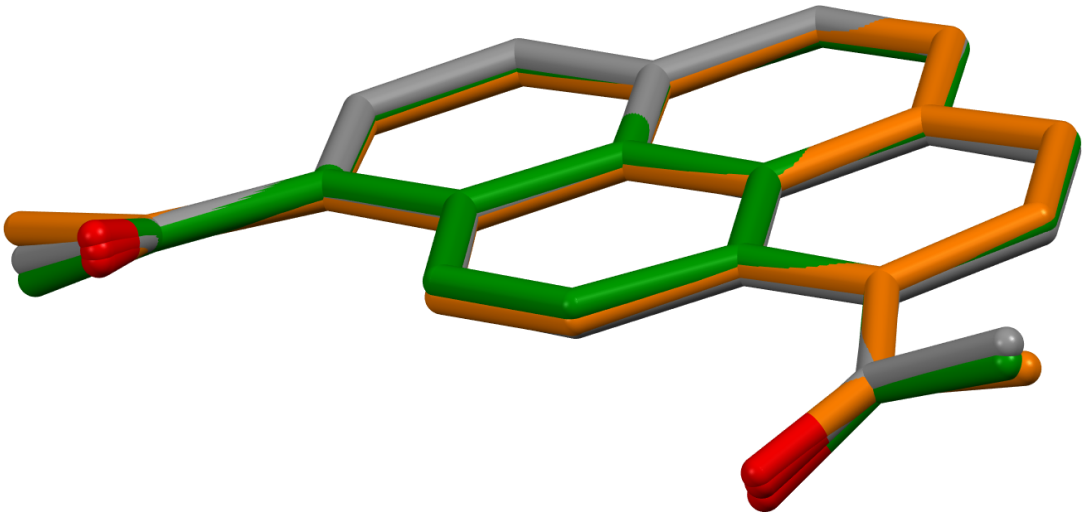

Figure S2.2: *Overlay of single molecules of 2"AP-α (green), 2"AP-β (orange) and free 2"AP molecule (gray) optimized in gas phase for the sake of electronic structure calculations. Due to the structural rigidity discussed in the main text, deviations between optimized and measured components do not exceed 0.3*Å*, while the RMSD between free molecule and α / β for overlay of all non-hydrogen atoms equals 0.0858*Å */ 0.0981*Å*, respectively. Hydrogen atoms have been omitted for clarity.*

Chapter S3

Lattice interactions

S3.1 The most important intermolecular interactions

Estimation of intermolecular interaction energy for all 2"AP crystal forms have been performed in CrystalExplorer17, [M. J. Turner et al., 2017] using cluster DFT/B3LYP calculations and standard 6-31G** database. The cluster included all molecules whose closest distance to central molecule was below 3.8Å. Initial geometry in all cases was based on crystal structures optimized in 0GPa and 0K using CRYSTAL17 software. [Dovesi et al., 2018]

Apart from investigated central moiety, the cluster of all four crystal forms included 14 symmetry related molecules: 9 independent ones in case of 2"AP-α, γ, and δ, and 4 independent ones in case of 2"AP-β. While technically it included also a fifteenth molecule in the case of the δ polymorph, this moiety was disregarded for the sake of further analysis due to lack of easily explainable interaction path, relatively large distance, and neglectible strength of interaction with the central moiety. This moiety was also absent in otherwise analogous clusters of 2"AP-α and 2"AP-γ.

Obtained values of interaction energy, summarized in Tables S3.1 and S3.2 unsurprisingly identifies π-stacking interaction to be crucial for overall sample stability in all investigated cases. It should be noted that all interaction featuring potential attraction between acetyl moieties are significantly attractive. Values consistently below -10kJ mol^{-1} suggest that the side chains aren't only responsible for steric repulsion, but rather play an active role in stabilizing the overall crystal structure.

While individual values output by CrystalExplorer can not be directly translated into lattice energy, a sum of interactions between one molecules and its neighbors should correlate well with the value of cohesive energy from periodic calculations. Since in all cases the cluster consists of 14 molecules, the average interaction strengths should be comparable and reflect the importance of intermolecular forces in each case. Based on this assumption we can see that the δ polymorph indeed benefits from adopting unfavorable molecular conformation, as its average interaction energy is the most negative among four investigated cases. At the same time we have observed 2"AP-β's molecules to assume conformation very close to the optimized minimum, so naturally its average interaction strength is expected to be the lowest out of all four crystal forms.

Table S3.1: *Intermolecular interactions in 2"AP polymorphs α, γ, and δ found between molecules within 3.8Å range. The values have been estimated by Crystal Explorer based on crystal structures optimized in 0K and 0GPa.*

	main interaction	relative placement	related by	interaction energy \ kJ mol^{-1} 2"AP-α	2"AP-γ	2"AP-δ
I	π-stacking	same slab†	-1	-53.0	-32.9	-60.4
II	π-stacking	same slab†	-1	-45.7	-59.6	-49.9
III	π-stacking	same slab†	c	-40.7	-41.6	-38.2
IV	C$-$H$\cdots$O	next slab†	1	-24.3	-29.2	-24.0
V	C$-$H$\cdots$O	next slab†	-1	-18.6	-23.2	-22.3
VI	C$-$H$\cdots$O	next slab†	c	-14.5	-10.5	-12.8
VII	C$-$H$\cdots$H$-$C	same ribbon	2_1	-11.2	-11.8	-12.0
VIII	C$-$H$\cdots$H$-$C	next slab†	2_1	-8.2	-10.4	-8.0
IX	C$-$H$\cdots$H$-$C	next slab†	-1	-0.5	-2.5	-1.0
X*	O$\cdots$O	next slab†	-1	–	–	+0.8
Average interaction energy within slab†				-33.8	-33.2	-35.1*
Average interaction energy between slabs†				-14.1	-15.7	-14.1*
Average interaction energy in overall				-22.5	-23.2	-23.1*

**X has been excluded from average interaction energy calculations*

† *"slab" denotes a 2D "brick-layer" stack of molecules infinite along* ***X*** *and* ***Y***

Table S3.2: *Intermolecular interactions in 2"AP polymorph β found between molecules within 3.8Å range. The values have been estimated by Crystal Explorer based on crystal structures optimized in 0K and 0GPa.*

	main interaction	relative placement	related by	interaction energy \ kJ mol^{-1} 2"AP-β
XI	π-stacking	same stack	1	-60.0
XII	C$-$H$\cdots$O	next stack	F	-18.2
XIII	C$-$H$\cdots$O	next stack	d	-15.5
XIV	C$-$H$\cdots\pi$	next stack	d	-5.1
Average interaction energy within stack				-60.0
Average interaction energy between stacks				-12.9
Average interaction energy in overall				-19.7

Chapter S4

Distinct spectroscopic properties of 2"AP polymorphs

S4.1 Luminescence of 2"AP in the solid state

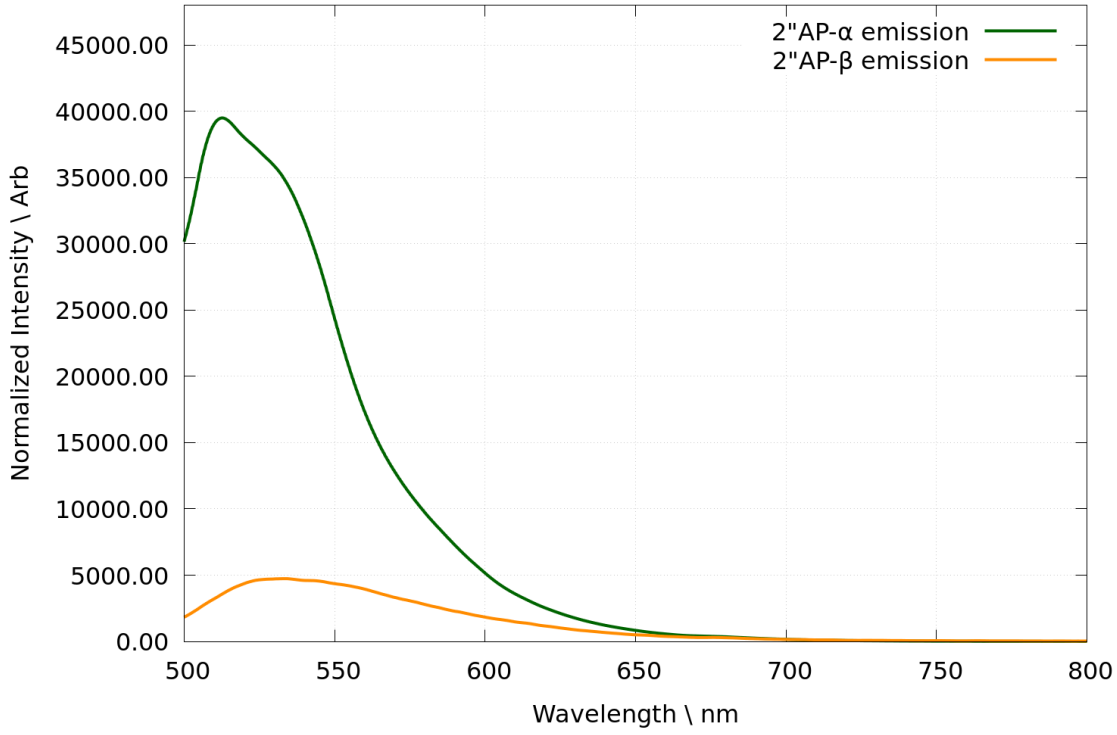

Figure S4.1: *Steady state excitation and fluorescence spectra of 2"AP α and β single crystals under ambient conditions. Excitation spectra were recorded at 515 nm and 535 nm for α and β samples accordingly, while both emission spectra were recorded at 475 nm. Intensities were registered for single crystals of comparable same size at the same experimental conditions (i.e.: the same intensity of the source, same filter / diaphragm settings and the same size of the irradiated area on the crystal).*

S4.2 Fluorescence decay curves

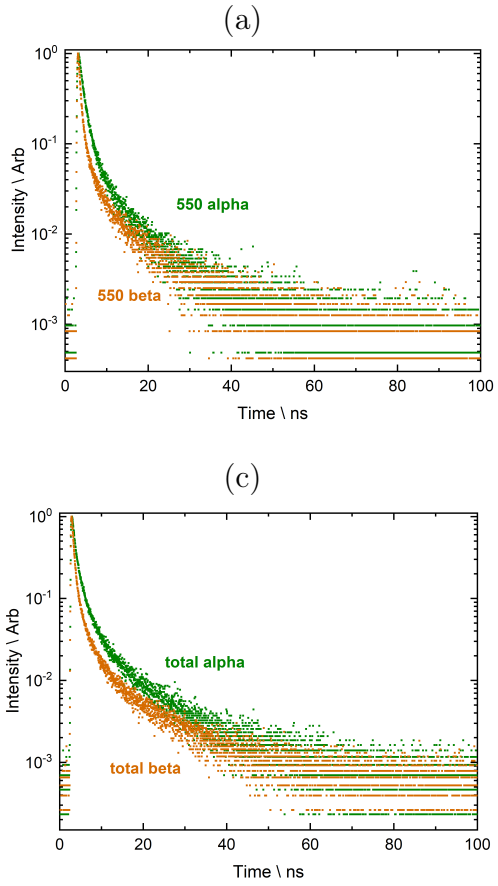

Figure S4.2: *2"AP fluorescence decay curves collected at (a) 550nm, (b) 600nm and (c) total range. Wavelength of choice was selected using adequate pass filters with 40nm FWHM positioned in front of detection system. Times of decay determined by the means of fitting a three-component decay curve, presented in Table 3, suggest the decay to be marginally slower at higher wavelengths.*

S4.3 Solid-state Raman spectra - a detailed band assignment

Raman spectra of the studied polymorphic structures of 2"AP were collected in order to examine differences in the crystals on a molecular level (Figure 4 in the manuscript). Both spectra exhibit several strong bands in the range between 1200 cm^{-1} and 1700 cm^{-1}. For the α polymorph, the most prominent ones are situated at 1229, 1377, 1592 and 1620 cm^{-1} and can be assigned to various ring vibrations. [Carrasco et al., 2003, Xie et al., 2010, Gu et al., 2013] The band at 1229 cm^{-1} comes from CH bending vibrations which are usually found between 1000 and 1300 cm^{-1}. Another interesting spectral region in the spectra of aromatic hydrocarbons is the 1350-1500 cm^{-1} range, where strong CH in-plane bending coupled with weak ring breathing modes are manifested. While a few bands in this area can be distinguished, the one at 1377 cm^{-1} has the highest intensity. Subsequently, we attribute several bands in the 1550-1650 cm^{-1} region, namely 1568, 1592, 1602 and 1619 cm^{-1}, to ring-stretching vibrations with some contribution of CH in-plane bending. Finally, the position of the remaining band of medium intensity at 1671 cm^{-1} is characteristic to carbonyl group vibration, observed e.g. in acetophenone and other aromatic derivatives. [Jayaraj et al., 1996, Sajan et al., 2006]

S4.4 Fluorescence as a function of pressure

Table S4.1: *Listing of fluorescence peak positions as a function of pressure. The values were obtained by fitting a gauss curve to the highest peak of each spectrum.*

pressure \ GPa	peak position \ nm	pressure \ GPa	peak position \ nm	pressure \ GPa	peak position \ nm
2"AP-α		2"AP-δ		2"AP-β	
0.00	519.79	1.61	572.41	0.00	538.47
0.27	534.52	2.24	586.69	0.81	582.65
0.50	539.40	2.55	599.30	1.25	592.58
0.74	544.34	2.99	614.47	1.93	605.05
0.90	545.30	3.36	622.32	2.39	613.83
		3.83	627.62	2.93	622.04
		4.15	635.30	3.02	628.28
		4.70	643.60	3.56	635.22
				3.92	641.76

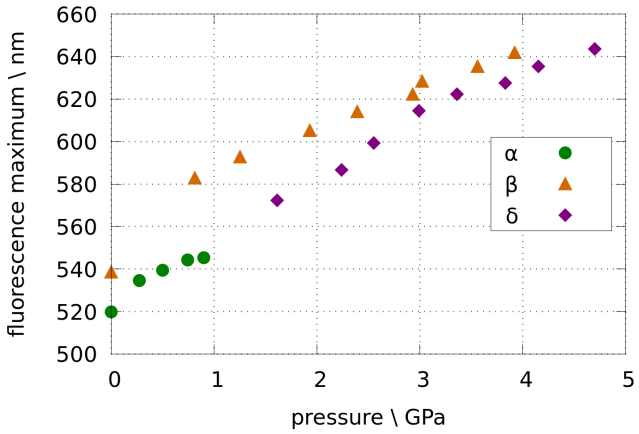

Figure S4.3: *Visualisation of fluorescence peak positions as a function of pressure. The values were obtained by fitting a gauss curve to the highest peak of each spectrum.*

S4.5 Comments on the former works regarding spectroscopic properties of 2"AP in the solid state

There were some major inconsistencies concerning solid state fluorescence study in the publication of Rajagopal et.al [Rajagopal et al., 2014]. Photographs of UV-illuminated crystals of 2"AP in that work (Scheme 1) indicate that:

a in the case of compounds 2AP and 2'AP luminescence is blue and green (i.e. with maxima around 450 and 525 nm accordingly) contrary to solid-state luminescence maxima of 602 and 567 nm reported in Table S7 and Figure S12,

b the sample marked as 2"AP luminesces in green, consistent with current study and inconsistent with Table S7,

c in the part concerning 2"AP luminescence in solution the maxima are given at 413 and 535 nm, whereas spectra in Figure S10 d suggest maxima 413 and 435 nm,

d in the case if 2"AP the samples under visible and UV illumination are clearly not the same.

Chapter S5

Theoretical calculations

S5.1 Conformational landscape of 2"AP

The analysis of 2"AP's conformational landscape was performed in CRYSTAL17, using dispersion-corrected DFT and 6-31G** basis set. The truncation criteria parameters were increased slightly. Contrary to previously described periodic calculations, these optimizations were performed using redundant internal parameters. This was necessary to impose restraints on values of two dihedral angles: δ_1 (O1 – C17 – C1 – C2) and δ_2 (O2 – C19 – C6 – C5), which were then both varied in range from -35° to 35° every 5 degrees. While scans with more intermediate coordinate values and larger scanning range were attempted, they included points which did not converge and as such were discontinued.

The procedure was found to depend on optimization path. Structures with the same dihedral constraints but different starting points were found to differ in final values of conformational stress by up to 15%. For that reason the scanning procedure was repeated four times using different optimization paths each time. Two starting geometries were obtained by optimizing an experiment-derived structure with restraints imposed on the values of dihedral angles: $\delta_1 = \delta_2 = +35°$ in one, $\delta_1 = \delta_2 = -35°$ in another. The scanning was then performed by varying one variable slowly and changing the other rapidly, as visualised in Figure S5.5.

The results were further corrected for molecule's internal symmetry: since in individual molecule acetyl moieties are indistinguishable, switching their labels should not influence final result. The same goes for positive and negative angle values, as rotation of individual group in both directions introduced analogous changes. Because of these symmetry restraints, values for the following pairs: $(\delta_1; \delta_2)$, $(\delta_2; \delta_1)$, $(-\delta_1; -\delta_2)$ and $(-\delta_2; -\delta_1)$ should be theoretically identical. Averaging energy values on those points and rescaling them so that minimum equals 0 yields final results described in main text.

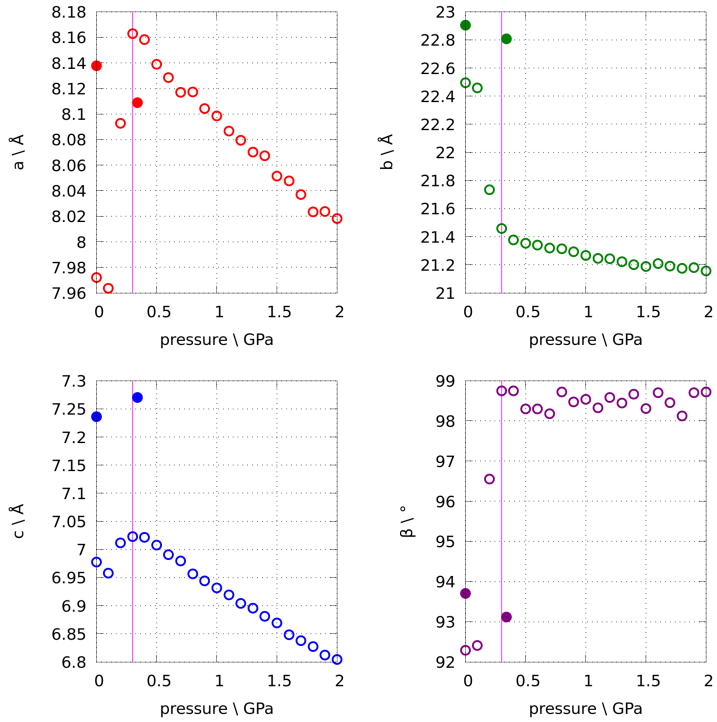

Figure S5.1: *Evolution of 2"AP-α's experimental (full circles) and optimized (empty circles) unit cell parameters with exerted pressure. Note that above 0.3GPa (pink line) the parameters match those of δ due to* in silico *phase transition.*

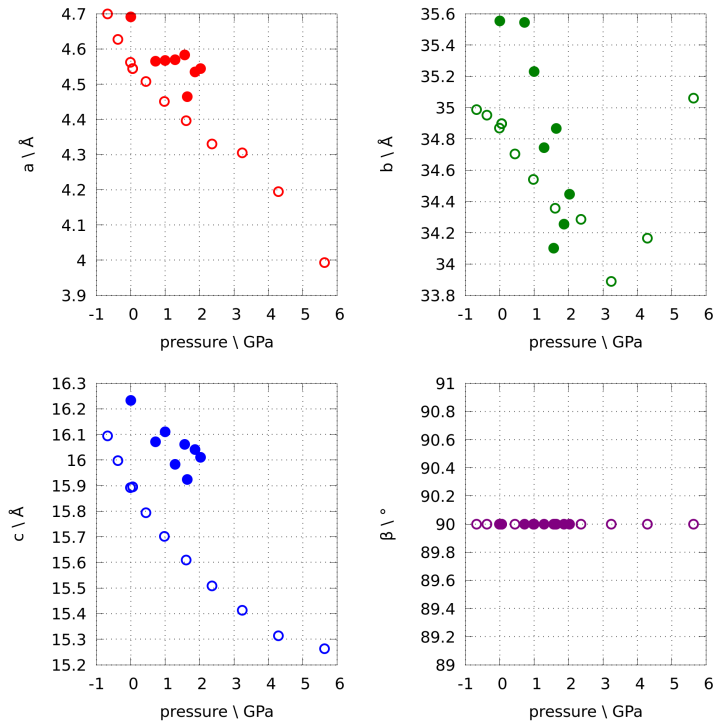

Figure S5.2: *Evolution of 2"AP-β's experimental (full circles) and optimized (empty circles) unit cell parameters with exerted pressure.*

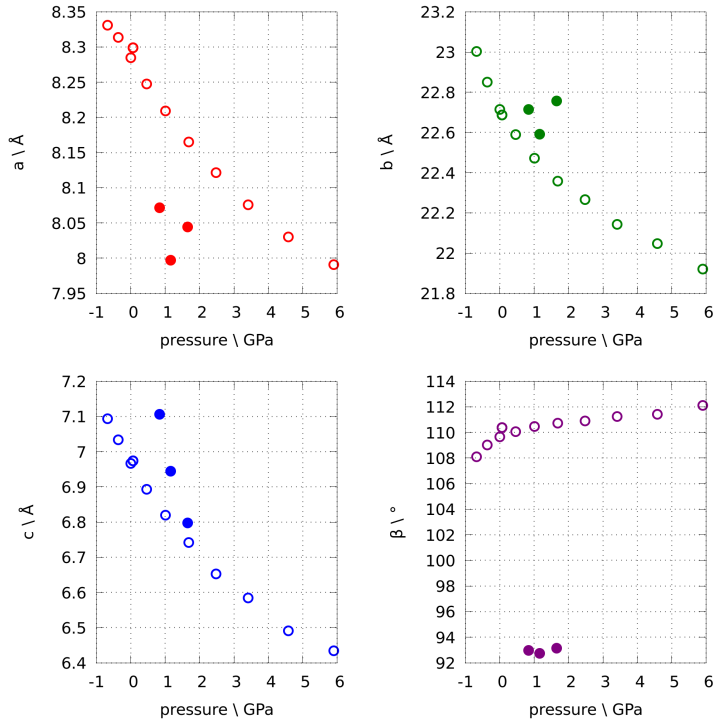

Figure S5.3: *Evolution of 2"AP-γ's experimental (full circles) and optimized (empty circles) unit cell parameters with exerted pressure.*

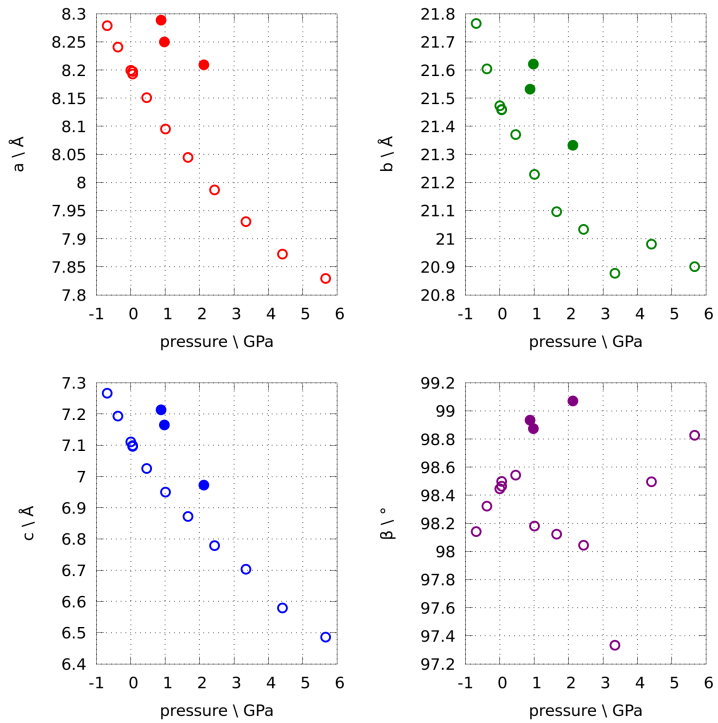

Figure S5.4: *Evolution of 2"AP-δ's experimental (full circles) and optimized (empty circles) unit cell parameters with exerted pressure.*

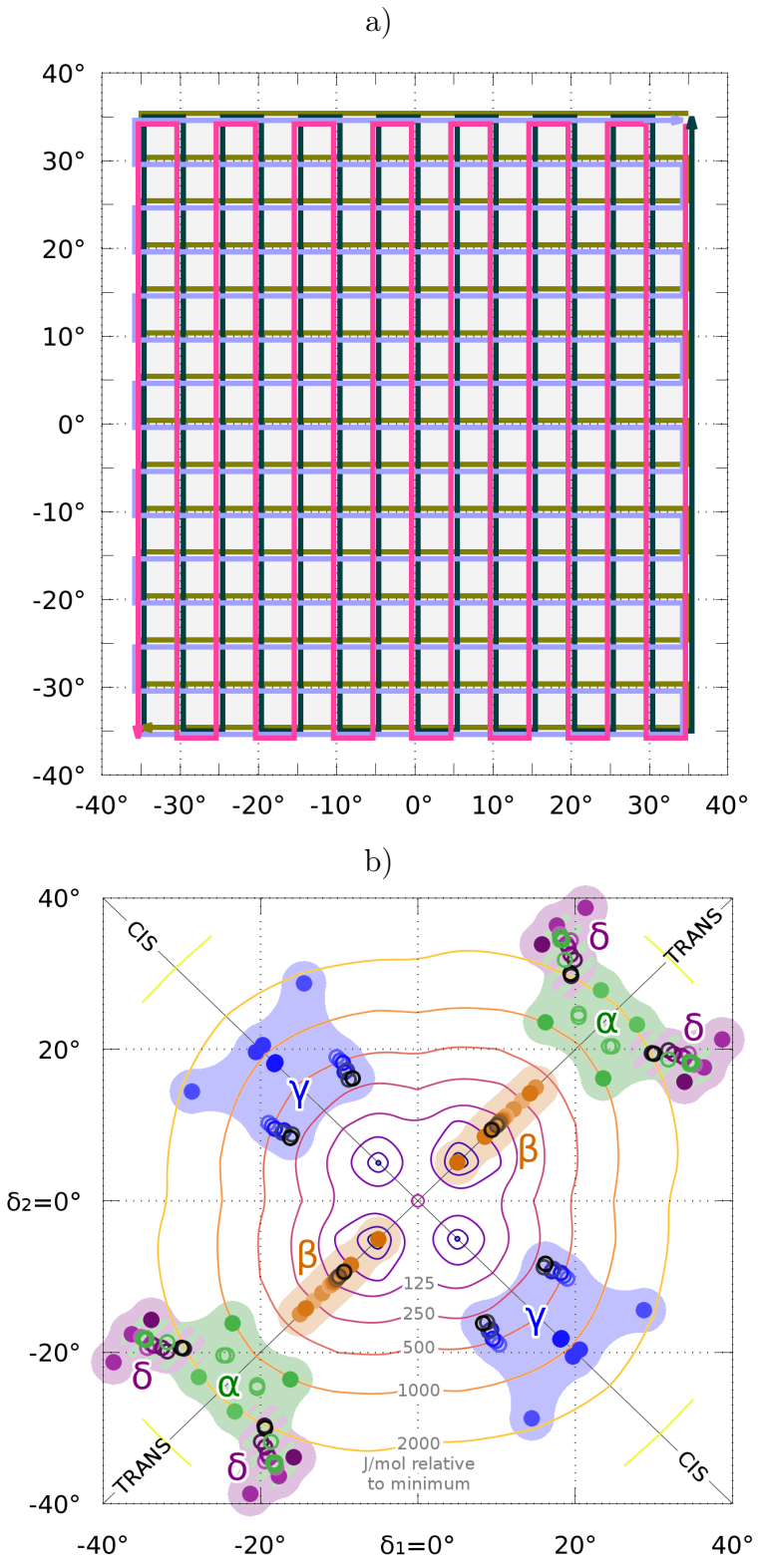

Figure S5.5: *a) Four scanning paths (coloured gold, violet, magenta and dark green) used to obtain values of conformational energy in investigated δ_1–δ_2 range. b) Potential energy landscape figure from main text repeated for reference.*

S5.2 Electronic excitations in 2"AP

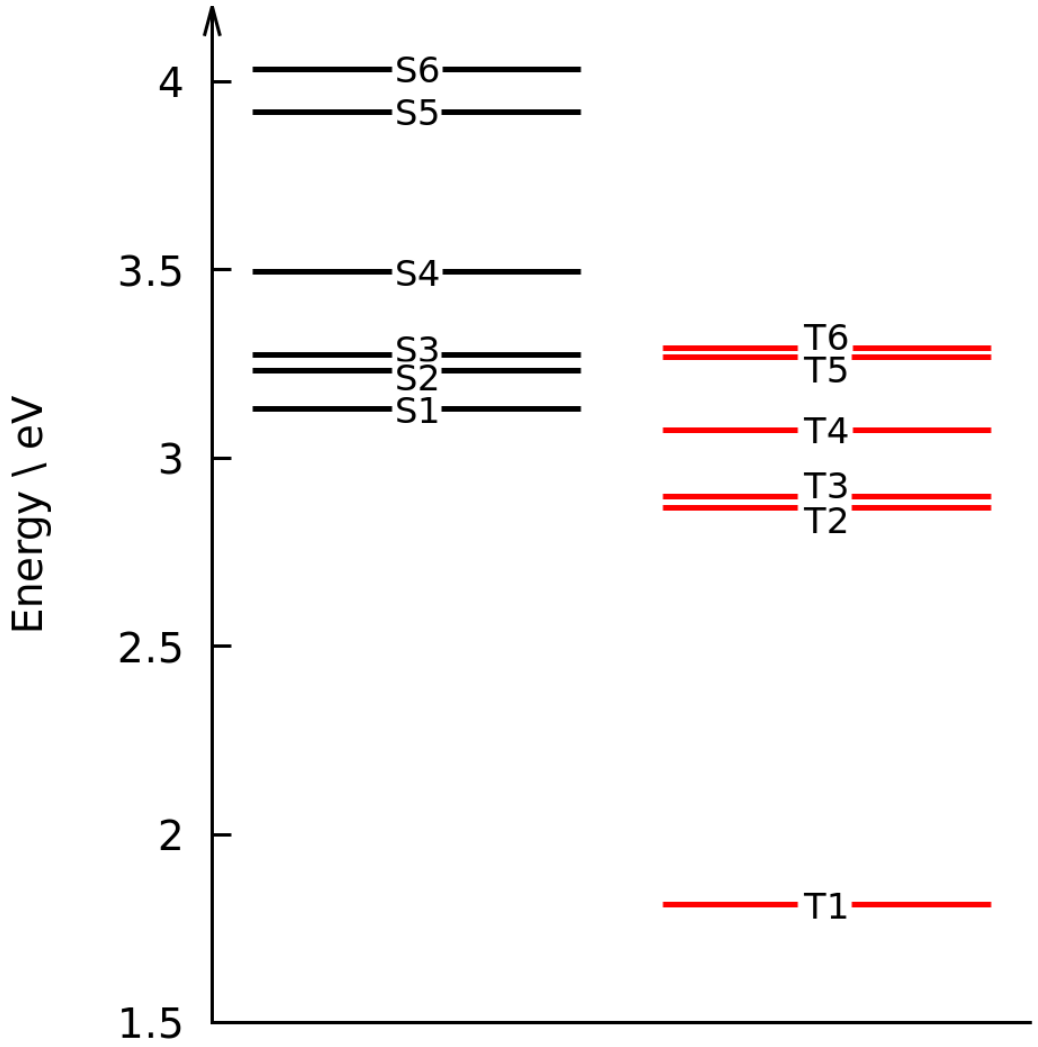

Figure S5.6: *Energy level diagram for molecular 2"AP. Excited singlet states represented in black, while triplet states - in red.*

Table S5.1: *Excitation energy, oscillator strength, main transition orbital, and their contribution calculated for molecular 2"AP using TD-DFT (B3LYP/6-311G**).*

Excitation		Main transition orbitals		Contribution \ %	ΔE \ eV	λ \ nm	f
S0 → S6		H → L+1	π → π*	0.60	4.0339	307.36	0.1703
S0 → S5		H-4 → L	π → π*	0.96	3.9201	316.27	0.0194
S0 → S4		H-3 → L	n → π* / π → π*	0.39	3.4949	354.76	0.0028
		H → L+1	π → π*	0.32			
		H-2 → L	n → π* / π → π*	0.24			
	S0 → T6	H-4 → L	π → π*	0.75	3.2914	376.69	0
S0 → S3		H-2 → L	n → π* / π → π*	0.52	3.2741	378.68	0.0001
		H-3 → L	n → π* / π → π*	0.36			
	S0 → T5	H → L+1	π → π*	0.68	3.2697	379.19	0
S0 → S2		H-1 → L	n → π*	0.88	3.2316	383.66	0.0044
S0 → S1		H → L	π → π*	0.94	3.1303	396.07	0.4224
	S0 → T4	H-3 → L	n → π* / π → π*	0.45	3.0743	403.29	0
		H-2 → L	n → π* / π → π*	0.38			
	S0 → T3	H-2 → L	n → π* / π → π*	0.47	2.8973	427.93	0
		H-3 → L	n → π* / π → π*	0.27			
	S0 → T2	H-1 → L	n → π*	0.76	2.8674	432.39	0
	S0 → T1	H → L	π → π*	0.95	1.8124	684.09	0

Table S5.2: *DFT-derived energy values corresponding to molecular orbitals of 2"AP presented in Figure 6 in main text.*

Orbital	Character	Energy \ eV
LUMO+1	π*	-1.74
LUMO	π*	-2.82
HOMO	π	-6.12
HOMO-1	n	-6.98
HOMO-2	n/π	-6.99
HOMO-3	n/π	-7.09
HOMO-4	π	-7.50

S5.3 Band gaps

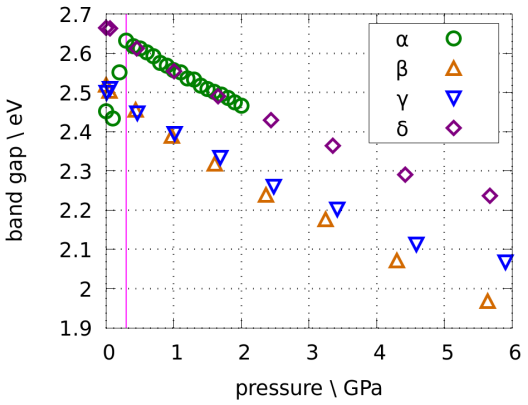

Figure S5.7: *Evolution of calculated band gap for four discussed 2"AP crystal forms. Values for the α phase were probed more densely and show the moment of its* in-silico *phase transfer to 2"AP-δ around 0.2 GPa.*

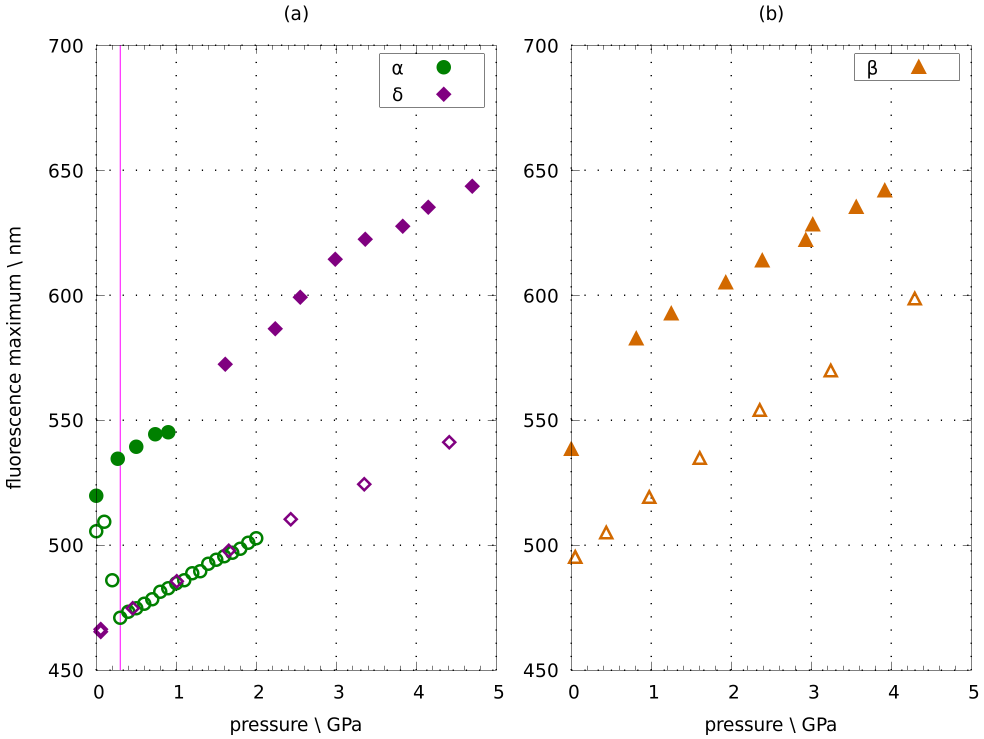

Figure S5.8: *Comparison of emission wavelength obtained by fitting a Gauss curve to experimental spectra (Figure S4.3, full points) and excitation wavelength from theoretical band gap span (Figure S5.7, hollow points). Note that above 0.3GPa (pink line) optimised values for α match those of δ due to* in silico *phase transition.*

Table S5.3: *Band gap extent and resulting hypothetical peak absorption wavelength calculated in CRYSTAL17 as a function of pressure. Presented band gap values have been also visualized in Figure S5.7.*

Pressure \ GPa	Band Gap \ eV	Calculated absorption \ nm
2"AP-α		
0	2.4519	505.67
0.1	2.4337	509.45
0.2	2.5511	486.00
0.3	2.6322	471.03
0.4	2.6185	473.49
0.5	2.6115	474.76
0.6	2.6018	476.53
0.7	2.5921	478.32
0.8	2.5751	481.47
0.9	2.5684	482.73
1	2.5574	484.81
1.1	2.5512	485.98
1.2	2.5363	488.84
1.3	2.5327	489.53
1.4	2.5170	492.59
1.5	2.5092	494.12
1.6	2.5017	495.60
1.7	2.4942	497.09
1.8	2.4862	498.69
1.9	2.4747	501.01
2	2.4657	502.84
2"AP-β		
0.00	2.5182	492.35
0.05	2.5035	495.24
0.44	2.4552	504.99
0.97	2.3876	519.28
1.61	2.3181	534.85
2.36	2.2383	553.92
3.25	2.1762	569.73
4.40	2.0713	598.58
5.64	1.9675	630.16

Pressure \ GPa	Band Gap \ eV	Calculated absorption \ nm
2"AP-γ		
0.00	2.5001	495.92
0.06	2.5102	493.92
0.46	2.4485	506.37
1.01	2.3952	517.64
1.68	2.3347	531.05
2.48	2.2610	548.36
3.42	2.2021	563.03
4.59	2.1135	586.63
5.90	2.0685	599.39
2"AP-δ		
0.00	2.6651	465.21
0.06	2.6636	465.48
0.46	2.6116	474.74
1.00	2.5536	485.53
1.66	2.4906	497.81
2.43	2.4294	510.35
3.35	2.3644	524.38
4.42	2.2908	541.23
5.67	2.2361	554.47

Chapter S6

Bibliography

[Bowskill et al., 2021] Bowskill, D. H., Sugden, I. J., Adjiman, C. S., and Pantelides, C. C. (2021). A reliable and efficient parameter estimation methodology for crystal structure prediction. part 1: Transferable models consistent with point charges. (in preparation).

[Bowskill et al., 2020] Bowskill, D. H., Sugden, I. J., George, N., Keates, A., Webb, J., Pantelides, C. C., and Adjiman, C. S. (2020). Efficient Parameterization of a Surrogate Model of Molecular Interactions in Crystals. In Pierucci, S., Manenti, F., Bozzano, G. L., and Manca, D., editors, *Computer Aided Chemical Engineering*, volume 48 of *30 European Symposium on Computer Aided Process Engineering*, pages 493–498. Elsevier.

[Carrasco et al., 2003] Carrasco, E. A., Campos-Vallette, M., Leyton, P., Diaz, G., Clavijo, R. E., García-Ramos, J. V., Inostroza, N., Domingo, C., Sanchez-Cortes, S., and Koch, R. (2003). Study of the interaction of pollutant nitro polycyclic aromatic hydrocarbons with different metallic surfaces by surface-enhanced vibrational spectroscopy (sers and seir). *The Journal of Physical Chemistry A*, 107(45):9611–9619.

[Dovesi et al., 2018] Dovesi, R., Erba, A., Orlando, R., Zicovich-Wilson, C. M., Civalleri, B., Maschio, L., Rérat, M., Casassa, S., Baima, J., Salustro, S., and Kirtman, B. (2018). Quantum-mechanical condensed matter simulations with CRYSTAL. *Wiley Interdisciplinary Reviews: Computational Molecular Science*, 8(4):e1360.

[Erba et al., 2014] Erba, A., Mahmoud, A., Belmonte, D., and Dovesi, R. (2014). High pressure elastic properties of minerals from ab initio simulations: The case of pyrope, grossular and andradite silicate garnets. *J. Chem. Phys.*, 140(12):124703.

[Frisch et al., 2016] Frisch, M. J., Trucks, G. W., Schlegel, H. B., Scuseria, G. E., Robb, M. A., Cheeseman, J. R., Scalmani, G., Barone, V., Petersson, G. A., Nakatsuji, H., Li, X., Caricato, M., Marenich, A. V., Bloino, J., Janesko, B. G., Gomperts, R., Mennucci, B., Hratchian, H. P., Ortiz, J. V., Izmaylov, A. F., Sonnenberg, J. L., Williams-Young, D., Ding, F., Lipparini, F., Egidi, F., Goings, J., Peng, B., Petrone, A., Henderson, T., Ranasinghe, D., Zakrzewski, V. G., Gao,

J., Rega, N., Zheng, G., Liang, W., Hada, M., Ehara, M., Toyota, K., Fukuda, R., Hasegawa, J., Ishida, M., Nakajima, T., Honda, Y., Kitao, O., Nakai, H., Vreven, T., Throssell, K., Montgomery, Jr., J. A., Peralta, J. E., Ogliaro, F., Bearpark, M. J., Heyd, J. J., Brothers, E. N., Kudin, K. N., Staroverov, V. N., Keith, T. A., Kobayashi, R., Normand, J., Raghavachari, K., Rendell, A. P., Burant, J. C., Iyengar, S. S., Tomasi, J., Cossi, M., Millam, J. M., Klene, M., Adamo, C., Cammi, R., Ochterski, J. W., Martin, R. L., Morokuma, K., Farkas, O., Foresman, J. B., and Fox, D. J. (2016). Gaussian 16 Revision C.01. Gaussian Inc. Wallingford CT.

[Groom et al., 2016] Groom, C. R., Bruno, I. J., Lightfoot, M. P., and Ward, S. C. (2016). The Cambridge Structural Database. *Acta Crystallographica Section B*, 72(2):171–179.

[Gu et al., 2013] Gu, X., Tian, S., Zhou, Q., Adkins, J., Gu, Z., Li, X., and Zheng, J. (2013). Sers detection of polycyclic aromatic hydrocarbons on a bowl-shaped silver cavity substrate. *RSC Adv.*, 3:25989–25996.

[Hafner, 2008] Hafner, J. (2008). Ab-initio simulations of materials using VASP: Density-functional theory and beyond. *Journal of Computational Chemistry*, 29(13):2044–2078.

[Jayaraj et al., 1996] Jayaraj, S. E., Ramakrishnan, V., Perumal, S., and Gurunathan, M. (1996). Surface enhanced raman scattering studies of acetophenone on colloidal silver particles. *Journal of Physics*, 47(3):255–259.

[Kazantsev et al., 2011] Kazantsev, A. V., Karamertzanis, P. G., Adjiman, C. S., and Pantelides, C. C. (2011). Efficient Handling of Molecular Flexibility in Lattice Energy Minimization of Organic Crystals. *Journal of Chemical Theory and Computation*, 7(6):1998–2016.

[M. J. Turner et al., 2017] M. J. Turner, J. J. McKinnon, S. K. Wolff, D. J. Grimwood, P. R. Spackman, D. Jayatilaka, and M. A. Spackman (2017). CrystalExplorer17 (2017).

[Merrill and Bassett, 1974] Merrill, L. and Bassett, W. A. (1974). Miniature diamond anvil pressure cell for single crystal x-ray diffraction studies. *Review of Scientific Instruments*, 45(2):290–294.

[Piermarini et al., 1975] Piermarini, G. J., Block, S., Barnett, J. D., and Forman, R. A. (1975). Calibration of the pressure dependence of the R_1 ruby fluorescence line to 195 kbar. *Journal of Applied Physics*, 46(6):2774–2780.

[Ragan et al., 1992] Ragan, D. D., Gustavsen, R., and Schiferl, D. (1992). Calibration of the ruby R1 and R2 fluorescence shifts as a function of temperature from 0 to 600 K. *Journal of Applied Physics*, 72(12):5539–5544.

[Rajagopal et al., 2014] Rajagopal, S. K., Philip, A. M., Nagarajan, K., and Hariharan, M. (2014). Progressive acylation of pyrene engineers solid state packing

and colour via C–H$\cdots$H–C, C–H$\cdots$O and π–π interactions. *Chemical Communications*, 50(63):8644–8647.

[Sajan et al., 2006] Sajan, D., Joe, I. H., and Jayakumar, V. S. (2006). Nir-ft raman, ft-ir and surface-enhanced raman scattering spectra of organic nonlinear optic material: p-hydroxy acetophenone. *Journal of Raman Spectroscopy*, 37(4):508–519.

[Sugden et al., 2016] Sugden, I., Adjiman, C. S., and Pantelides, C. C. (2016). Accurate and efficient representation of intramolecular energy in ab initio generation of crystal structures. I. Adaptive local approximate models. *Acta Crystallographica Section B: Structural Science, Crystal Engineering and Materials*, 72(6):864–874.

[Tchoń and Makal, 2021] Tchoń, D. and Makal, A. (2021). Software for rapid and reproducible pressure determination based on ruby chip fluorescence - pruby. (in preparation).

[Vinet et al., 1987] Vinet, P., Smith, J. R., Ferrante, J., and Rose, J. H. (1987). Temperature effects on the universal equation of state of solids. *Phys. Rev. B*, 35(4):1945–1953.

[Xie et al., 2010] Xie, Y., Wang, X., Han, X., Xue, X., Ji, W., Qi, Z., Liu, J., Zhao, B., and Ozaki, Y. (2010). Sensing of polycyclic aromatic hydrocarbons with cyclodextrin inclusion complexes on silver nanoparticles by surface-enhanced raman scattering. *Analyst*, 135:1389–1394.